Experimental testing and model validation of the calcination of calcium carbonate by the reduction of copper oxide with CH_4

José Ramón Fernández*, Juan Carlos Abanades

Spanish Research Council, INCAR-CSIC, Francisco Pintado Fe, n. 26 (33011) Oviedo (Spain)

*jramon@incar.csic.es

Abstract

The reduction reaction of copper oxide with CH_4 is highly exothermic and can be arranged to generate sufficient heat to in-situ calcine calcium carbonate and produce a highly concentrated stream of CO_2. This concept is tested at TRL4 in a packed-bed reactor operated close to adiabatic conditions. The impact of the initial solids temperature and the inlet flowrate of the gases is evaluated. A 50/50 (vol.%) mixture of methane and hydrogen (i.e., a possible composition of the PSA-off gas generated in a reforming process) has also been used as reducing gas. The presence of H_2 reduces the $CuO/CaCO_3$ proportion required in the bed and promotes the calcination at temperatures lower than 870 ºC. The experimental measurements are well predicted by a one-dimensional fixed-bed reactor model, in which the steam methane reforming, water-gas-shift, carbon deposition and carbon gasification reactions are also considered. Different characterization techniques (i.e., SEM, XRD, N_2 adsorption, TPR) demonstrate that both commercial CuO- and CaO-based materials show good stability after successive cyclic experiments.

Keywords: CO_2 capture; chemical looping; calcium looping; H_2 production, $CaCO_3$ calcination; CuO reduction

1. Introduction

There is a growing concern about the need to cut down the emissions of CO_2 from industrial and power generation sectors with the purpose of reducing the effects of climate change (IPCC, 2014). CO_2 capture and storage should play a crucial role in a severe diminution of the emissions of carbon dioxide far beyond the limit nowadays achieved in the industries powered by fossil fuels, and thus achieve the objectives recently established at COP22 held in Marrakech (i.e., 50% reduction of CO_2 emissions by 2050 and 100% by 2100) with the aim of keeping the rise in global mean temperature below 1.5 ºC (IEA, 2017). The deployment of highly-efficient pre-

combustion systems for the capture of CO_2 is a sustainable alternative to produce H_2 with a low carbon footprint (Boot-Handford et al., 2014). About 95% of hydrogen is nowadays produced from fossil sources while emitting roughly 0.5 Gt of CO_2 pear year (Voldsun et al., 2016). Moreover, the global demand for H_2 will increase in the coming decades because of the rise in the ammonia and methanol production, the growing use of hydrogen in refineries, steel and chemical plants and also to the role of H_2 as a sustainable fuel in recent applications (such as fuel cells, novel gas turbines, etc) (IEA, 2015). Steam Methane Reforming (SMR) combined with water-gas-shift (WGS) units is still the dominant method to produce hydrogen at a large scale (i.e., almost 50% of total H_2 production) (IEA, 2015). However, the energy-intensive steam methane reforming requires for a large amount of additional energy to accomplish the endothermic conversion of methane into H_2, thereby producing a significantly high amount of CO_2 (about 7 kg CO_2/kg H_2) (Rostrup Nielsen, 2009).

The Sorption Enhanced Reforming (SER) is an intensified technology that combines SMR with the rapid separation of CO_2 by using a sorbent material (typically a CaO-based solid) (Hufton et al., 1999). The simultaneous removal of CO_2 from the gaseous phase promotes the production of H_2 according to the Le Chatelier's principle (Harrison, 2008). Therefore, virtually pure H_2 (i.e. between 90 and 96 vol.% H_2, dry basis) is produced in a single reaction step operated at temperatures between 650 and 700 ºC, in contrast to the typical temperature range of 900-1000 ºC for conventional SMR (Antzara et al., 2016). Moreover, the exothermic carbonation of CaO compensates for the endothermic SMR enthalpy, thereby avoiding the addition of more energy to the process (Diglio et al., 2018).

The principal issue that hinders the scaling-up of the SER technology is the need to decrease the energy penalty due to the sorbent calcination stage, which requires temperatures of around 900 ºC under CO_2-rich atmospheres (Baker, 1962). Of the different process schemes that have so far been proposed for reducing the energy penalty, only the oxy-fuel combustion (Shimizu et al., 1999) has been validated at a large pilot-plant scale in post-combustion applications up to TRL6-7 (Arias et al. 2013; Strohle et al., 2014). The chemical looping combustion (CLC) technology has been also considered for the calcination of calcium carbonate in an attempt to avoid the energy consuming and costly Air Separation Unit needed for oxy-combustion processes (Lyon and Cole, 2000). In a CLC system, a metal oxide, generally referred as to oxygen carrier

(OC), is subjected to a redox cycling (Ishida and Jin, 1994). The lattice O_2 reacts with the fuel producing virtually pure CO_2 (after the removal of H_2O), suitable for transport, storage or for other industrial purposes (Adanez et al., 2012). Once the oxygen carrier is reduced, it is subsequently oxidized in a second stage by reacting with air. In the CLC concept, the CO_2 is obtained separately since the combustion gases are obtained avoiding their dilution with N_2 (Lyngfelt, 2018). Different CLC configurations using fluidized beds have been envisaged to provide the heat required for the regeneration of the calcium-based sorbent by placing the carbonated particles in contact with oxygen carriers that have been previously heated up to temperatures above 1000 ºC in an oxidation reactor (Wolf and Yan, 2005; Fernández and Abanades, 2016; Fernández and Abanades, 2017a). General Electric initially proposed the idea of carrying out both the oxidation of the reduced O_2 carrier and the $CaCO_3$ calcination in one step, which should increase the energy efficiency (Lyon and Cole, 2000). However, this is not a CO_2 capture process since the oxidation is carried out with air, and consequently, the carbon dioxide is emitted highly diluted with nitrogen.

In the calcium-copper looping process, the necessary heat to calcine $CaCO_3$ is supplied by the reduction of copper oxide with a fuel gas (Abanades et al., 2010). With this chemical loop process it is possible to obtain separate streams of virtually pure H_2, N_2 and CO_2, as can be seen in Fig. 1. The calcium-copper looping process follows a sequence of 3 reaction steps (Fernández et al., 2012a). A H_2-rich gas is first obtained through the SER of CH_4, where the reactor contains a reforming catalyst, a Cu-based material that acts as inert in this stage, and a CaO-based sorbent, which is carbonated (Fernández et al., 2012b). The Cu-based solid is subsequently oxidized with diluted air to moderate the maximum bed temperature and avoid the partial calcinacion of $CaCO_3$ (Fernández et al., 2014). In the third stage, the calcium carbonate formed during the SER is calcined thanks to the heat supplied by the reduction of the CuO-based solid with a gaseous fuel (mainly methane or the PSA-off gas obtained from the SER stage). An appropriate proportion of copper oxide and calcium carbonate ensures that the heat generated during the CuO reduction is sufficient to decompose completely the calcium carbonate without extra supply of energy (Alarcón and Fernández, 2015). In contrast to the previous stages that are favoured at high pressures, the reduction/calcination stage must be accomplished at atmospheric pressure to make possible the calcination reaction

between 850 ºC and 910 ºC, so as to decrease the demand of energy and minimize the sintering of the solids.

The calcium-copper looping process has been mainly envisaged to be performed in configurations of several packed-bed reactors operating in parallel (Fernández et al., 2012a). In these systems, the solids remain steady and the inlet gas is repeatedly switched between SER, oxidizing and reducing conditions. Fixed-bed reactors do not require solids filtering systems located downstream, since the formation of fines by attrition is avoided, and they allow the operation to take place at a high pressure, which results in a more compact design. Moreover, H_2 and N_2 can be produced at a suitable pressure to facilitate their subsequent use in industrial applications and/or power generation (Martínez et al., 2013; Martínez et al., 2014; Martini et al., 2017a; Fernández et al., 2017; Martínez et al., 2017).

An important progress has been carried out over the last years in the deployment of the calcium-copper looping process (Fernández and Abanades, 2017b). Various reactor models based on those developed for packed-bed chemical looping systems (Han et al., 2013; Hamers et al., 2014; Fernández and Abanades, 2014; Spallina et al., 2015), were reported to represent the dynamic performance of every stage of the process (Fernández et al., 2012b; Fernández and Abanades 2014; Alarcón and Fernández, 2015; Qin et al., 2016) and to devise operation strategies aimed at reducing the number of reactors, increasing the amount of CO_2 captured and avoiding undesirable side reactions (Martini et al., 2016; Fernández and Abanades, 2017c; Martini et al., 2017b). Furthermore, a large number of works about novel synthetic solids suitable for Ca-Cu applications have been reported. Synthetic calcium-based sorbents (Martavaltzi et al., 2011; Valverde et al., 2012; Broda et al, 2013; Zhenissova et al., 2014), hybrid reforming catalyst-CaO materials (Martavaltzi and Lemonidou, 2010; García-Lario et al., 2015; Aloisi et al., 2017) and CaO-CuO composites (Manovic and Anthony, 2011; Kierzkowska and Müller, 2012; Rahman et al., 2015; Kazi et al., 2017) have shown a good reactivity and stable performance after multiple cycles. The feasibility of the reaction steps described in Fig. 1 has been experimentally confirmed in packed-bed reactors at laboratory scale during the recent FP7 project, ASCENT. The operational limits of a reforming catalyst mixed with a CaO-based solid after several SER and redox cycles were evaluated (Grasa et al., 2017). Alarcón et al. (2017) experimentally demonstrated that the dilution of air with recycled N_2 moderates the temperature reached during the copper oxidation,

so that the calcinacion of calcium carbonate is partially avoided. Moreover, the calcination of calcium carbonate by the in situ reduction of CuO has been successfully demonstrated with mixtures of hydrogen and carbon monoxide (Fernández et al., 2016; Alarcón et al., 2017).

In the present work, the key reaction stage of the calcium-copper looping process, i.e., the simultaneous CuO reduction/$CaCO_3$ calcination, is demonstrated using methane as reducing gas in a pilot fixed-bed reactor at TRL4. Different ranges of operating variables including the initial temperature of the bed and the inlet flow rate are investigated. The morphology of the copper- and calcium-based solids has been studied by using different characterization techniques. A dynamic reactor model has been developed to represent the evolution of the composition of the product gas and of the bed temperature during the experiments.

2. Material and methods

2.1. Experimental setup

The core of the experimental setup consisted of a tubular reactor made of Inconel (L=1 m, ID=0.038 m). Johnson Matthey and Carmeuse supplied the functional solids for the experimental campaign. A homogeneous mixture of about 1060 g, composed of a CuO-based material (65 wt.% CuO/SiO_2) and a calcium-based material (98 wt.% calcium oxide), was loaded in the reactor. The materials were first crushed and subsequently sieved to achieve an average size of around 0.003 m. The axial temperature profiles were measured in 15 points by K-type thermocouples. The metallic tube was insulated with a 0.15 m wide layer of quartz wool to minimize the loss of heat. A 14 kW ceramic furnace surrounded both the fixed bed and the cover of quartz wool in order to preheat the solids and compensate the heat loss during the reaction tests. The amount of heat supplied by the furnace was controlled by an additional thermocouple located half-way along the reactor-oven system. The gaseous feed was preheated by means of two heating-tapes each with a capacity of 800 W. Bronkhorst mass-flow controllers were used to regulate the gas flow rates and compositions of the feed. A tubular bed loaded with SiO_2 was located downstream of the reactor to remove the steam produced during the tests. Finally, the dry composition of the product gas was registered online with a SICK GMS810 analyser equipped with IR and thermal conductivity detectors. The tests were performed at atmospheric pressure. A scheme of the experimental setup is presented in Fig. 2.

The morphology of the materials was examined by scanning electron microscopy combined with energy-dispersive X-Ray analysis (SEM-EDX), by using a Quanta FEG 650 microscope equipped with an Ametek-EDAX analyser. The main crystalline features that appear in both the CaO- and CuO-based materials after multiple oxidation-carbonation-reduction/calcination tests were obtained by X-ray diffraction (XRD) on a powder diffractometer (Siemens D500/501) connected to a copper Kα monochromatic X-ray detector (2θ from 20º to 70º, step size=0.02º, scan time/step=1 s). The BET surface areas and pore volume distributions (BJH) have been calculated from N_2 adsorption measurements carried out at -196ºC in a Micromeritics ASAP-2460 apparatus. The reducibility and the reversibility of the CuO-based material after the multicycle operation were evaluated by temperature programmed reduction (TPR) measurements. The samples were placed in an AutoChemII Micromeritics apparatus and exposed to a 10 vol% H_2/Ar gas that was linearly heated at 10 ºC/min from 40 to 900 ºC.

2.2. **Fixed-bed reactor model**

The evolution of the composition of the outlet gas as well as the temperature profiles inside the reactor has been represented using a 1-D reactor model. A multicomponent system (composed of CH_4, CO_2, CO, H_2, CuO, Cu, $CaCO_3$, CaO, C and inert) has been modelled assuming axially dispersed plug flow, negligible inter-particle mass and temperature profiles, uniform void fraction in the solids bed ($\varepsilon = 0.5$) and the perfect distribution of the calcium- and copper-based solids along the bed. The variations of the physical properties with changes in composition and temperature have been considered in the model. Any gas-to-solid heat and mass transfer resistances, as well as radial temperature and concentration profiles are assumed to be negligible, since the system has been operated at relatively high flowrates (between 2 and 4 Nl/min) and a small packing size (d_p=0.003 m). Possible intra-particle diffusion resistances are assumed by including average effectiveness factors (η) in the kinetics. The reactor model also considers the heat-transfer between the fixed bed and the environment by means of an overall heat-transfer coefficient (U) included in the energy balance, which has been experimentally calculated. The description of the implementation of the reactor model in Matlab is detailed in previous works (Fernández et al., 2012c; Fernández et al., 2013). Table 1 presents an overview of the mass, energy, momentum balances as well as the equations used to calculate the axial mass and heat dispersion.

The reaction rate of CuO reduction with methane, hydrogen and carbon monoxide is described with a shrinking core model (SCM) limited by the chemical reaction. The SCM is also used for the calcination of $CaCO_3$, as in some previous works on modelling of CLC and calcium looping systems (García-Labiano et al., 2004; Martínez et al., 2012).

The copper-based solid may partially catalyze both the steam methane reforming and the water-gas-shift (WGS) reactions (Alarcón et al., 2017) (steam is present due to the oxidation of methane). The kinetics obtained by Xu and Froment (1989) have been assumed to describe these catalytic reactions. The presence of CaO in the bed should minimize the formation of carbon due to methane decomposition (Harrison, 2008). However, particles of previously reduced oxygen carrier may catalyze this reaction to some degree. For this reason, the kinetic correlation calculated for a Ni-Cu/MgO catalyst by Borghei et al. (2010) has been incorporated in the model. Moreover, carbon gasification may occur due to the presence of CO_2 and steam (Zhou et al., 2013). The kinetics proposed by Snoeck et al. (2002) for both gasification reactions have also been assumed. The kinetic equations used in this work are listed in Table 2.

3. Results and discussion

The fixed-bed reactor initially showed significant differences in temperature profile at temperatures higher than 500 ºC due to the large heat lost especially at the bottom of the bed (Fernández et al., 2016). Several modifications were carried to improve the insulation of the reactor, which mainly consisted of increasing the thickness of the quartz wool coating (from 8 to 15 mm) surrounding the metallic tube. Afterwards, several heat-transfer tests were carried out to calculate the overall heat-transfer coefficient (U) of the new arrangement. About 40 Nl/min of nitrogen was fed into the fixed bed that contained about 1 kg of Al_2O_3 (particle diameter of 0.003 m). First, the solids bed was heated up from ambient temperature to 470 ºC by means of preheated gas. In another experiment, the solids initially at 500 ºC were cooled by feeding in nitrogen at 300 ºC. The pseudo-homogeneous model described above (in which the terms related to the chemical reactions are omitted) was used to fit the experimental temperature profiles and a value of 2.5 W/m^2K was estimated for U. These results demonstrate that the experimental setup operates near adiabatic conditions. The results obtained during the heating experiment are represented in Fig. 3.

During the experimental tests, about 25 cycles were carried out in the fixed-bed reactor following a sequence of reduction/calcination, oxidation and carbonation stages. Different characterization techniques were used to evaluate the stability of these materials. As can be seen in Fig. 4, the sample of fresh CaO-based material (i.e., before the cyclic experiments) exhibits large grains and low porosity. After the cyclic tests, the solid maintains its morphological structure, although it starts to show some sintering (Fig. 4b). The copper-based sample initially shows a highly porous structure with large CuO-rich grains (Fig. 4c). There are not perceptible signs of sintering in the copper-based material after the cycles (Fig. 4d). SEM-EDX analyses reveal the presence of Cu in certain zones of the cycled CaO-based sample (e.g. site B in Fig. 4b). The results are presented in Table 3.

XRD analyses were made to study the crystallinity of the functional Ca-Cu solids and to detect possible variations in the chemical composition of these materials after 25 cycles. As shown in Fig. 5, small quantities of combined Ca-Cu oxides formed in both the Ca- and Cu-based solids after the experiments. These combined oxides may have formed due to the high operating temperatures achieved during the reduction/calcination tests. However, no Cu_2O was found in the aged CuO-based material (Fig. 5b), which demonstrates the absence of O_2 uncoupling during the reduction/calcination operation even at temperatures above 900 ºC. The formation of hybrid Ca-Cu compounds may have slightly affected the O_2 transport capacity of the OC and the CO_2 sorption capacity of the calcium-based sorbent, as reported in previous works (Kierzkowska and Müller, 2012; Alarcón et al., 2017), although confirmation of this is outside the scope of this study.

Both BET pore surface area and the BJH pore volume distribution of the fresh materials are represented in Fig. 6. The BET surface area (157 m^2/g) and the pore volume (0.28 cm^3/g) are higher than the typical values obtained for CuO-rich oxygen carriers (Imtiaz et al., 2012; García-Lario et al., 2013). The pore size distribution presents two peaks at 1 and 4 nm. The calcium-based solid shows a significantly lower BET surface area (i.e., 11 m^2/g), although this value corresponds to that obtained for other CaO-based solids (Kierzkowska and Müller, 2012). The pore volume is also significantly lower than that of the copper-based sample (i. e. 0.025 cm^3/g). The pore size distribution of the fresh CO_2 sorbent shows a pronounced peak at 9 nm. Minor variations are detected in the textural characteristics of the cycled oxygen carrier. The BET surface area and the BJH pore volume slightly decrease to 135 m^2/g and 0.21 cm^3/g, respectively, and their pore

diameter distributions are very similar. In the case of the used calcium-based solid, its textural properties remain virtually unaltered (i.e, the BET surface area is about 9 m^2/g and the BJH pore volume 0.01 cm^3/g, without any change in the pore size distribution).

Temperature-programmed reduction (TPR) tests confirm the high stability of the O_2 carrier after successive cycles. As can be seen in Fig. 7, a solitary peak between 180 and 280 ºC is obtained for two samples of fresh and aged CuO-based material, which corresponds to the consumption of hydrogen during the reduction of CuO. The area under the curve for both samples is very similar, which indicates that the amount of active CuO in the solid remains stable after the experimental campaign performed in the fixed-bed reactor. About 0.47-0.49 mmol H_2 were consumed in these analyses, which approximately correspond to a total reduction of the CuO present in the samples.

For the reduction/calcination experiments, the fixed-bed reactor was initially heated in air up to 600 ºC. Then, a stream of pure CO_2 (5 Nl/min) preheated to 600 ºC was fed into the solids bed for 30 min to partially carbonate the CaO-based particles in order to ensure an appropriate proportion of CuO and $CaCO_3$ in the reactor. After the carbonation step, the $CaCO_3$ content in the fixed bed should be about 10 wt.% (together with 27 wt.% of CuO), according to previous studies carried out in TGA with this material (Alarcón et al., 2017). The rest of the bed corresponds to silica (which is the inert binder of the copper-based solid) and inert CaO. At these conditions, the copper oxide/carbonate molar ratio present in the bed is around 3.2, which should be enough to accomplish the reduction/calcination operation with methane without additional energy supply (Alarcón and Fernández, 2015) (i.e., the ceramic oven is only necessary to compensate for the heat loss in the experimental setup). As the calcium particles were progressively carbonated, the reactor was also heated up to reach a bed temperature between 610 ºC at the bottom and approximately 800 ºC at the upper part of the reactor (for a pre-set temperature in the oven of about 780 ºC).

To reduce the CuO, a flowrate of 3 Nl/min of methane at 620 °C was fed into the reactor. The experimental measurements of the temperature profiles and the gas compositions as well as the predictions with the reactor model are presented in Fig. 8. As the reduction of the CuO particles with CH_4 progresses, the temperature of the reactor increases. However, the increase in temperature observed in the first part of the reactor is significantly lower than that measured in a previous work where the tests were accomplished with the same material using H_2 and CO as reducing gases (Alarcón et al.,

2017). This demonstrates that the reactivity of methane with copper oxide is modest at temperatures below 750 ºC. During the first 3 minutes, the maximum temperature is lower than 840 °C, which impedes the calcination of the calcium carbonate. As a result, during this period of time, the carbon dioxide measured at the reactor exit corresponds entirely to the oxidation of methane.

The heat exchanged between the inlet gas and the converted solids generates a heat front which advances along the bed together with the reduction front. The relative positions of both fronts mainly depend on the composition of the reacting gas and the amount of active component in the oxygen carrier (Noorman et al., 2007). Since the content of CH_4 in the feed is high and there is a low percentage of active CuO in this particular solids mixture, the reduction reaction front is moving ahead of the heat transfer front. As a result, the solids bed already traversed by the reduction front is left at a high temperature, so that the CH_4 reaches the reduction front already preheated. After 45 minutes, the bed achieves a maximum temperature of around 900 ºC, leading to a fast calcination of $CaCO_3$ and increasing concentrations of CO_2 at the reactor exit of up to 93 vol. %, on a dry basis. As shown in Fig. 8b, the reactor model gives an accurate description of the evolution of the temperature profiles in the vast majority of the bed. The maximum temperatures achieved at any time are reasonably well predicted, which indicates that both Ca- and Cu-based solids are uniformly distributed along the bed. Hot spots would have been detected in those parts of the reactor with excessive amount of CuO. Only at the end of the bed a significant difference can be discerned ,which is probably caused by heat losses in that region. This phenomenon has been underestimated by the reactor model (there is an overall heat-transfer coefficient calculated by the entire solid bed), giving rise to higher theoretical temperatures compared to those obtained experimentally.

In the period of time between t=2 min and t=5 min, the methane achieves almost total conversion (pre-breakthrough), but from that moment on, the methane concentration in the product gas gradually increases during a long breakthrough period, which is extended up to 26 min, as a consequence of the low reactivity of CuO with CH_4. Moreover, an increasing amount of CO is measured during the breakthrough period. The high temperature, the presence of $H_2O_{(v)}$ from the oxidation of CH_4 and the high concentration of CO_2 favour the steam methane reforming and then the reverse water-gas-shift reaction, both of which are catalysed by the reduced copper-based solids. As

332 explained in section 2.2., a certain degree of carbon deposition may appear where the
333 copper-based particles have already been reduced. The presence of CO_2 and steam may
334 promote the gasification of the deposits of C, thereby contributing to the formation of
335 CO during the pre-breakthrough period. When the oxygen carrier approaches total
336 reduction, the temperature profile decreases progressively and the concentration of CO
337 at the reactor exit increases until a nearly constant value of 8 vol.% is achieved.

338 Once the dynamic model has been validated, it is possible to estimate theoretically the
339 evolution of the solids conversion throughout the reactor. As shown in Fig. 8c, the
340 reduction of CuO with CH_4 does not take place in a sharp reaction front, especially
341 during the first minutes of the operation, where the temperatures in the bed are
342 relatively low. The calcination of $CaCO_3$ is then hindered, and as a result, the reduction
343 front moves forward faster than the calcination zone (in contrast to the
344 reduction/calcination tests performed with H_2 or mixtures of H_2/CO, in which both
345 fronts move forward together (Alarcón et al., 2017). After 2 minutes of operation, about
346 40% of maximum CuO conversion has been achieved in the first third of the bed and
347 the amount of $CaCO_3$ calcined is negligible. However, from t=5 min onwards, when the
348 solids bed achieves a maximum temperature of around 900 ºC, the calcination is
349 favoured and a considerable fraction of the carbonated solids in this region of the
350 reactor is completely calcined. After 10 minutes of operation, the CuO-based solids are
351 approaching total conversion, whereas the carbonated particles located in the second
352 part of the bed achieve conversions of between 55% and 60%. From the theoretical
353 evolution of the calcination profiles (X_CaCO_3), it was possible to estimate the flow of
354 CO_2 that corresponds exclusively to the calcination of the sorbent (represented in Fig.
355 8a as "CO_2 from calci"). In view of these results, about 1.3 moles of methane (which
356 corresponds to 3 Nl/min fed into the reactor for 10 min) were necessary to decompose
357 about 0.53 moles of calcium carbonate (for the conditions of this test).

358 After the reduction/calcination operation, diluted air was used to carry out the oxidation
359 of the oxygen carrier at temperatures lower than 850ºC. Afterwards, pure CO_2 was
360 introduced to re-carbonate the calcium-based particles following the procedure
361 explained above, leaving the bed ready to initiate a new cycle.

362 Additional experiments were performed to evaluate the influence of the initial bed
363 temperature on the CuO reduction/$CaCO_3$ calcination operation. These experiments
364 were initiated with average bed temperatures of between 700 ºC and 800 ºC,

maintaining the rest of the conditions of the reference case explained above. As can be seen in Fig. 9, the bed temperature at the beginning of the experiment has a decisive effect on the concentration and temperature profiles. When the reduction/calcination is initiated with a temperature in the reactor of about 700 ºC, the increase in temperature along the bed is modest because the reduction of copper oxide with CH_4 is hampered. The maximum temperature achieved does not exceed 820 ºC after 5 min of operation. From that moment onwards, the bed temperature progressively decreases up to reach temperatures between 700 and 800 ºC for t=10 min. Therefore most of the $CaCO_3$ is left uncalcined. In these conditions, almost all the CO_2 must come from the oxidation of CH_4. From the very beginning, the conversion of the gas is low and concentrations of methane at the reactor exit above 20 vol.% are observed. After 3 minutes, the methane content gradually increases reaching a value of about 80% (t=18 minutes). The low temperature also impedes both steam methane reforming and reverse WGS reactions, resulting in concentrations of CO and H_2 below 1 vol.% during the breakthrough.

The temperature and product gas composition change significantly when the experiment starts with higher temperatures in the bed. The reduction of copper oxide with CH_4 is promoted and a larger increase in temperature is then obtained ($\Delta T \approx 100$ ºC in the upper part of the reactor). When the reduction/calcination starts with a bed temperature of about 800 ºC (on average), the fuel gas is almost completely converted during the first 4 minutes (i.e., <3 vol.% of CH_4 measured at the reactor exit) and virtually pure CO_2 (dry basis) predominates during the pre-breakthrough. Temperature profiles above 900 ºC in the second half of the bed are obtained in these conditions, which should facilitate the decomposition of $CaCO_3$ in the upper part of the reactor. A maximum temperature of about 930 ºC is achieved after 5 min of operation. From then on, the temperature declines because the CuO particles approach total reduction and bed temperatures of between 860 and 905 ºC are measured in the second part of the reactor for t=10 min.

During the breakthrough period, the concentration of CH_4 progressively increases due to the fact that the copper-based particles are close to total reduction. Meanwhile, the contents of carbon monoxide and hydrogen in the product gas also increase because the higher temperatures registered during this period promote the steam methane reforming, WGS and carbon gasification reactions (during the pre-breakthrough carbon monoxide and hydrogen not observed in the product gas because they react with CuO as soon as they are produced). As shown in Fig. 9, the reactor model describes reasonably well the

experimental measurements, especially those obtained in the experiments performed at higher temperatures.

Following the evolution of the solids conversion (not shown here for the sake of simplicity), it can be observed that both the reduction and calcination fronts advance closer when the test is carried out with an average starting temperature in the reactor of about 800 ºC. After 10 minutes of experiment (i.e., when the CuO particles have been totally reduced), about 60% of the $CaCO_3$ has been calcined (reaching maximum carbonate conversions of about 70-75% in the second part of the bed). This means that about 1.3 moles of methane (which corresponds to 3 Nl/min fed into the reactor for 10 min) were necessary to decompose around 0.64 moles of calcium carbonate. In view of these results, the operation at higher temperature increased 20% the amount of $CaCO_3$ calcined.

The influence of the inlet flowrate on the solids bed temperature and on the composition of the product gas was also analysed (starting with a bed temperature of around 760 ºC, on average). Streams of pure methane from 2 Nl/min to 4 Nl/min were fed into the fixed-bed reactor. As shown in Fig. 10, low flow rates of methane allowed a sufficient residence time of the CH_4 inside the bed to be almost completely converted to CO_2 and steam during the first few minutes of operation. The heat released from the CuO reduction led to a further increase in the temperature until it reached maximum values of 895 ºC and 905 ºC after 10 minutes of operation for 2 and 3 Nl/min, respectively. With 4 Nl/min, the residence time of the gas was insufficient to achieve total conversion of CH_4 for the conditions of the experiment. The higher inlet flow of methane accelerated the advance of the reduction front and a maximum temperature of 875 ºC was already achieved for t=5 min. From that moment onwards, the bed was progressively cooled down to temperatures below 850 ºC after 10 minutes of operation. During the pre-breakthrough period, more than 10 vol.% of CH_4 was obtained and a smaller concentration of CO_2 was measured, as a result of the lower degree of CH_4 oxidation and $CaCO_3$ calcination achieved.

Finally, 2 Nl/min made up of 50 vol% of CH_4 and 50 vol% of H_2 and preheated at 620 ºC was fed into the bed to accomplish the reduction/calcination operation. This composition may correspond to a typical PSA off-gas from a purifying stage of the H_2-rich product of a SER process (Martínez et al., 2014). Taking into account the composition of the fuel gas, a copper/calcium molar ratio of 2.5 is needed in the reactor

to allow for an operation under thermally neutral conditions. First, a carbonation stage with pure CO_2 was carried out for 1 hour to increase the amount of $CaCO_3$ in the bed. This is the period of time estimated to achieve the degree of carbonation in the CO_2-sorbent on the basis of previous TGA experiments (Alarcón et al., 2017). Before the reduction/calcination test, the reactor was heated until it reached a temperature close to that of the first experiment (Fig. 8) carried out with CH_4 (i.e., with an average temperature in the solids of around 760 ºC).

As shown in Fig. 11, the presence of H_2 in the feed prolongs the time required to achieve the total reduction of the bed to around 20 minutes (1 mole of CH_4 reduces 4 moles of CuO, whereas the reduction of CuO with H_2 is an equimolar reaction). The great reactivity of CuO with hydrogen facilitates a fast increase in bed temperature to a maximum of 830 ºC in the first 5 minutes of the test. The hydrogen is oxidized to $H_2O_{(v)}$ inside the bed, which considerably reduces the partial pressure of CO_2. As a result, a relatively fast $CaCO_3$ calcination is feasible from t=10 min onwards, which is the period of time with temperatures in the reactor between 850 ºC and 890 ºC. During part of the pre-breakthrough period, the fuel gases are totally converted and almost pure CO_2 is obtained (i.e., about 98 vol.% CO_2, dry basis). Although the reactor model describes reasonably well the experimental temperature during most of the reduction/calcination operation, higher temperatures are predicted at the end of the bed when the CuO-based particles are close to be totally reduced (i.e., during the breakthrough and post-breakthrough periods). The reactor model seems to underestimate the heat loss in that region when the Cu reduction does not supply heat to the bed anymore. In view of the evolution of the solids conversion profiles (not shown in Fig. 11 for the sake of simplicity), about 1.8 moles of reducing gas (50/50 of CH_4 and H_2) were necessary to decompose about 0.77 moles of $CaCO_3$. These results indicate that the use of 50% of H_2 instead of CH_4 increased about 45% the amount of CaCO3 calcined. Once the CuO-based particles are totally reduced, the fixed bed behaves like a catalytic reactor, where the main reactions are steam methane reforming and WGS favoured by the high temperatures still present in the bed. As a result, a gas containing about 42 vol.% CH_4, 35 vol.% H_2 and 13 vol.% CO is obtained.

As explained above, the Ca-Cu materials used in this work have been subjected to about 25 cycles during the experimental tests. Different characterization techniques showed that the chemical composition and textural properties of both solids remain virtually

unaltered after multicycle operation (see Figs. 4-7). Most of the series of experiments carried out in the fixed-bed reactor were repeated in order to confirm the stability of the materials in the long term. Fig. 12 show the outlet gas composition and the axial temperature profiles obtained during the cycle 1 and cycle 20 carried out with CH_4 in the feed (3 Nl/min) and 760 ºC of average starting temperature. As can be seen, both gas composition and temperature profiles are very similar, which demonstrates the high stability of both CaO- and CuO-based materials. In both cases, the solids bed achieves a maximum temperature above 900 ºC after 10 minutes of operation. During the pre-breakthrough (t<5 min), the methane is almost totally converted and only 4-5 vol.% CH_4 is measured. The amount of CO_2 registered in the product gas in both cycles is similar and the duration of the breakthrough period is around 20 min, which demonstrates that the reactivity of the solids remain stable during the cyclic operation.

Conclusions

The feasibility of the CuO reduction/$CaCO_3$ calcination operation has been evaluated in a packed-bed reactor at TRL4 operating close to adiabatic conditions. The impact of the starting temperature of the bed and the inlet gas flow rate on the operation has been evaluated. When the operation is carried out with initial temperatures in the reactor higher than 800 ºC, the reduction of CuO is favoured, resulting in the complete oxidation of the inlet CH_4 and the calcination of a large fraction of the calcium carbonate. In these conditions, virtually pure CO_2 is obtained during part of the pre-breakthrough period. In the particular experimental set up used in this work, low flow rates (i.e., lower than 3 Nl/min of CH_4) allow a sufficient residence time of the methane inside the reactor to be almost completely converted to carbon dioxide and steam. Temperature profiles higher than 900 ºC are then recorded and large amounts of CO_2 resulting from the oxidation of methane and the decomposition of the calcium carbonate are observed. The relatively long breakthrough periods demonstrate that the reactivity of the methane with the copper oxide is significantly lower than that measured of hydrogen. The reduced copper-based material partially catalyses the steam methane reforming, water-gas-shift, carbon deposition and carbon gasification reactions. When the bed is approaching total reduction, significant concentrations of carbon monoxide and hydrogen are measured. The dynamic reactor model used in this study describes reasonably well the experimental curves recorded. SEM, XRD, N_2 adsorption and TPR

497 analyses have demonstrated the good stability of the Ca-Cu solids after being subjected
498 to 25 redox/carbonation/calcination cycles.

499 **Acknowledgements**

500 The authors acknowledge the contribution of J.M Alarcon during the experimental
501 campaign. This research was funded by the EU-FP7 ASCENT Project (Grant agreement
502 number 608512).

503 **References**

504 Abanades, J.C., Murillo, R., Fernández, J.R., Grasa, G., Martínez, I., 2010. New CO_2 capture
505 process for hydrogen production combining Ca and Cu chemical loops. Environ. Sci. Technol.
506 44: 6901-6904.

507 Adánez, J., Abad, A., García-Labiano, F., Gayán, P., de Diego, L.F., 2012. Progress in
508 Chemical-Looping Combustion and Reforming technologies. Prog. Energ. Combust. 38, 215-
509 282.

510 Alarcón, J.M., Fernández, J.R., 2015. $CaCO_3$ calcination by the simultaneous reduction of CuO
511 in a Ca/Cu chemical looping process. Chem. Eng. Sci.137, 254−267.

512 Alarcón, J.M., Fernández, J.R., Abanades, J.C., 2017. Study of a Cu-CuO chemical loop for the
513 calcination of $CaCO_3$ in a fixed bed reactor. Chem. Eng. J. 325, 208-220.

514 Aloisi, I., Di Giuliano, A., Di Carlo, A., Foscolo, P.U., Courson, C., Gallucci, K., 2017.
515 Sorption enhanced catalytic steam methane reforming: experimental data and simulations
516 describing the behaviour of bi-functional particles. Chem. Eng. J. 314, 570-582.

517 Antzara, A., Heracleous, E., Lemonidou, A.A., 2016. Energy efficient sorption enhanced-
518 chemical looping methane reforming process for high-purity H_2 production: Experimental
519 proof-of-concept. Appl. Energ. 180, 457-471.

520 Arias, B., Diego, M.E., Abanades, J.C., Lorenzo, M., Diaz, L., Martinez, D., Alvarez, J.,
521 Sanchez-Biezma, A., 2013. Demonstration of steady state CO2 capture in a 1.7MWth calcium
522 looping pilot. Int. J. Greenh. Gas Con. 18, 237–245.

523 Baker, E.H., 1962. The calcium oxide-calcium dioxide system in the pressure range 1-300
524 atmospheres. J. Chem. Soc. 70, 464-470.

525 Boot-Handford, M.E., Abanades, J.C., Anthony, E.J., Blunt, M.J., Brandani, S., Mac Dowell,
526 N., Fernandez, J.R., Ferrari, M.C., Gross, R., Hallett, J.P., Haszeldine, R.S., Heptonstall, P.,
527 Lyngfelt, A., Makuch, Z., Mangano, E., Porter, R.T.J., Pourkashanian, M., Rochelle, G.T.,
528 Shah, N., Yao, J.G., Fennell, P.S., 2014. Carbon capture and storage update. Energ. Environ.
529 Sci.7, 130-189.

530 Borguei, M., Karimzadeh, R., Rashidi, A., Izadi, N., 2010. Kinetics of methane decomposition
531 to COx-free hydrogen and carbon nanofiber over Ni-Cu/MgO catalyst. Int. J. Hydrg. Energ. 35,
532 9479-9488.

Broda, M., Manovic, V., Imtiaz, Q., Kierzkowska, A., Anthony, E., Muller, C., 2013. High-purity hydrogen via the sorption-enhanced steam methane reforming reaction over a synthetic CaO based sorbent and a Ni catalyst. Environ. Sci. Technol. 47, 6007-6014.

Diglio, G., Hanak, D.P., Bareschino, P., Pepe, F., Montagnaro, F., Manovic, V., 2018. Modelling of sorption-enhanced steam methane reforming in a fixed bed reactor network integrated with fuel cell. Appl. Energ. 210, 1-15.

Edwards, M.F., Richardson, J.F., 1968. Gas dispersion in packed beds. Chem. Eng. Sci. 23, 109-123.

Fernández, J.R., Abanades, J.C., Murillo, R., Grasa, G., 2012. Conceptual design of a hydrogen production process from natural gas with CO_2 capture using a Ca–Cu chemical loop. Int. J. Greenh. Gas Con. 6, 126–141.

Fernández, J.R., Abanades, J.C., Grasa, G., 2012. Modeling of sorption enhanced steam methane reforming – Part II: simulation within a novel Ca/Cu chemical loop process for hydrogen production. Chem. Eng. Sci. 84, 12–20.

Fernandez, J.R., Abanades, J.C., Murillo, R., 2012. Modeling of sorption enhanced steam methane reforming in an adiabatic fixed bed reactor. Chem. Eng. Sci. 84, 1-11.

Fernandez, J.R., Abanades, J.C., Murillo, R., 2013. Modeling of Cu oxidation in adiabatic fixed-bed reactor with N2 recycling in a Ca/Cu chemical loop. Chem. Eng. J. 232, 442-452.

Fernández, J.R., Abanades, J.C., Murillo, R., 2014. Modeling of Cu oxidation in an adiabatic fixed-bed reactor with N2 recycling. Appl. Energ. 113, 1945-1951.

Fernández, J.R., Abanades, J.C., 2014. Conceptual design of a Ni-based chemical looping combustion process using fixed-beds. Appl. Energ. 135, 309-319.

Fernández, J.R., Abanades, J.C., 2016. CO_2 capture from the calcination of $CaCO_3$ using iron oxide as heat carrier. J. Clean. Prod. 112, 1211-1217.

Fernández, J.R., Alarcón, J.M., Abanades, J.C., 2016. Investigation of a Fixed-Bed Reactor for the Calcination of $CaCO_3$ by the Simultaneous Reduction of CuO with a Fuel Gas. Ind. Eng. Chem. Res. 55, 5128−5132.

Fernández, J.R., Abanades, J.C., 2017. Sorption enhanced reforming of methane combined with an iron oxide chemical loop for the production of hydrogen with CO_2 capture: Conceptual design and operation strategy. Appl. Thermal Eng. 125, 811‑822.

Fernández, J.R., Abanades, J.C., 2017. Overview of the Ca-Cu looping process for hydrogen production and/or power generation. Current Opinion Chem. Eng. 17, 1-8.

Fernández, J.R., Abanades, J.C., 2017. Optimized design and operation strategy of a Ca-Cu chemical looping process for hydrogen production. Chem. Eng. Sci. 166, 144–160.

Fernández, J.R., Martínez, I., Abanades, J.C., Romano, M.C., 2017. Conceptual design of a Ca-Cu chemical looping process for hydrogen production in integrated steelworks. Int. J. Hydrog. Energ. 42, 11023-11037.

García-Labiano, F., de Diego, L.F., Adánez, J., Abad, A., Gayán, P., 2004. Reduction and oxidation Kinetics of a copper-based oxygen carrier prepared by impregnation for chemical-looping combustion. Ind. Eng. Chem. Res. 43, 8168-8177.

Garcia-Lario, A.L., Martinez, I., Murillo, R., Grasa, G., Fernandez, J.R., Abanades, J.R., 2013. Reduction Kinetics of a High Load Cu-based Pellet Suitable for Ca/Cu Chemical Loops. Ind. Eng. Chem. Res. 52, 1481−1490.

Garcia-Lario, A.L., Grasa, G., Murillo, R., 2015. Performance of a combined CaO-based sorbent and catalyst on H_2 production, via sorption enhanced methane steam reforming. Chem. Eng. J. 264, 697-705.

Grasa, G., Navarro, M.V., López, J.M., Díez, L., Fernández, J.R., Murillo, R., 2017. Validation of the SER H_2 production stage under relevant conditions for the Ca/Cu process. Chem. Eng. J. 324, 266-278.

Gunn, D.J., Misbah, M.M.A., 1993. Bayesian estimation of heat transport parameters in fixed beds. Int. J. Heat Mass. Transf. 36, 2209-2221.

Gunn, D.J., 1978. Axial and radial dispersion in fixed beds. Chem. Eng. Sci. 42, 363-373.

Hamers, H.P., Gallucci, F., Cobden, P.D., Kimball, E., van Sint Annaland, M., 2014. CLC in packed beds using syngas and CuO/Al_2O_3: a model description and experimental validation. Appl. Energ. 119, 163-172.

Han, L., Zhou, Z., Bollas, G.M., 2013. Heterogeneous modeling of chemical-looping combustion. Part1: Reactor model. Chem. Eng. Sci. 104, 233–249.

Harrison, D.P., 2008. Sorption-enhanced hydrogen production: a review. Ind. Eng. Chem. Res. 47, 6486–501.

Hufton, J.R., Mayorga, S., Sircar, S., 1999. Sorption-enhanced reaction process for hydrogen production. AIChE J.45 (2), 248-256.

IEA, Technology Roadmap. Hydrogen and Fuel Cells. IEA Publications, Paris, France, 2015.

IEA, CO_2 emissions from fuel combustion, OECD/IEA, Paris, 2017.

IPCC- Climate Change 2014: Mitigation of Climate Change. Contribution of Working Group III to the Fifth Assessment Report of the Intergovernmental Panel on Climate Change. Cambridge University Press, Cambridge, United Kingdom and New York, NY, USA, 2014.

Imtiaz, Q., Kierzkowska, A.M., Broda, M., Müller, C.R., 2012. Synthesis of Cu-Rich, Al2O3-Stabilized Oxygen Carriers Using a Coprecipitation Technique: Redox and Carbon Formation Characteristics. Environ. Sci. Technol. 46, 3561−3566.

Ishida, M., Jin, H., 1994. A new advanced power-generation system using chemical-looping combustion. Energy 19, 415-422.

Kazi, S.S., Aranda, A., di Felice, L., Mayer, J., Murillo, R., Grasa, G., 2017. Development of cost effective and high performance composite for CO_2 capture in Ca–Cu looping process. Energy Procedia. 114,211–219.

607 Kierzkowska, A.M., Müller, C.R., 2012. Development of calcium-based, copper-functionalised
608 CO2 sorbents to integrate chemical looping combustion into calcium looping. Energ. Env. Sci.
609 5, 6061-6065.

610 Krupiczka, R., 1967. Analysis of thermal conductivity in granular materials. Int. Chem. Eng. 7,
611 122-144.

612 Lyngfelt, A., 2014. Chemical-looping combustion of solid fuels - Status of development. Appl.
613 Energ. 113, 1869-1873.

614 Lyon, R.K., Cole, J.A., 2000. Unmixed combustion: an alternative to fire. Combust. Flame 121,
615 249-261.

616 Manovic, V., Anthony, E.J., 2011. Integration of calcium and chemical looping combustion
617 using composite CaO/CuO-based materials. Environ. Sci. Technol. 45,10750-10756.

618 Martavaltzi, C.S., Lemonidou. A.A., 2010. Hydrogen production via sorption enhanced
619 reforming of methane: Development of a novel hybrid material-reforming catalyst and CO2
620 sorbent. Chem. Eng. Sci. 65, 4134-4140.

621 Martavaltzi, C., Pefkos, T.D., Lemonidou, A.A., 2011. Operational Window of Sorption
622 Enhanced Steam Reforming of Methane over CaO-Ca12Al14O33. Ind. Eng. Chem. Res. 50,
623 539–545.

624 Martínez, I., Grasa, G., Murillo, R., Arias, B., Abanades, J.C., 2012. Kinetics of calcination of
625 partially carbonated particles in a Ca-looping system for CO_2 capture. Energy Fuel. 26, 1432-
626 1440.

627 Martínez, I., Murillo, R., Grasa, G., Fernández, J.R., Abanades, J.C., 2013. Integrated combined
628 cycle from natural gas with CO_2 capture using a Ca-Cu chemical loop. AIChE J. 59, 2780-2794.

629 Martinez, I., Romano, M.C., Fernandez, J.R., Chiesa, P., Murillo, R., Abanades, J.C., 2014.
630 Process design of a hydrogen production plant from natural gas with CO_2 capture based on a
631 novel Ca/Cu chemical loop. Appl. Energ. 114,192−208.

632 Martinez, I., Armaroli, D., Gazzani, M., Romano, M.C, 2017. Integration of the Ca-Cu process
633 in Ammonia Production Plants. Ind. Eng. Chem. Res. 56, 2526-2539.

634 Martini, M. van den Berg, A., Gallucci, F., van Sint Annaland, M., 2016. Investigation of the
635 process operability windows for Ca-Cu looping for hydrogen production with CO_2 capture.
636 Chem. Eng. J. 303,73–88.

637 Martini, M., Martínez, I., Gallucci, F., Romano, M.C., Van Sint Annaland, M., 2017. Packed
638 Bed Ca-Cu Looping Process Integrated with a Natural Gas Combined Cycle for Low Emission
639 Power Production. Energy Procedia. 114, 104-112.

640 Martini, M., Martinez, I., Romano, M.C., Chiesa, P., Gallucci, F., van Sint Annaland., 2017.
641 Increasing the carbon capture efficiency of the Ca/Cu looping process for power production
642 with advanced process schemes. Chem. Eng. J.328, 304-319.

643 Noorman, S., van Sint Annaland, M., Kuipers, J.A.M., 2007. Packed bed reactor technology for
644 chemical-looping combustion. Ind. Eng. Chem. Res. 46, 4212–4220.

Qin, C., Yin, J., Feng, B., Ran, J., Zhang, L., Manovic, V., 2016. Modelling of the calcination behaviour of a uniformly-distributed $CuO/CaCO_3$ particle in Ca-Cu chemical looping. Appl. Energ. 164, 400-410.

Rahman, R.A., Mehrani, P., Lu, D.Y., Anthony, E.J., Macchi, A., 2015. Investigating the use of CaO/CuO sorbents for in situ CO_2 capture in a biomass gasifier. Energ Fuel. 29, 3808-3819.

Rostrup-Nielsen, J.R., 2009. Steam reforming and chemical recuperation. Catal. Today 145, 72-75.

Shimizu ,T., Hirama, T., Hosoda, H., Kitano, K., Inagaki, M., Tejima, K., 1999. A twin fluid-bed reactor for removal of CO_2 from combustion processes. Chem. Eng. Res. Des. 77, 62-69.

Snoeck, J.W., Froment, G.F., Fowles, M., 2002. Steam/CO2 reforming of methane. Carbon filament formation by the boudouard reaction and gasification by CO2, by H2, and by steam: kinetic study. Ind. Eng. Chem. Res. 41, 4252– 4265.

Spallina, V., Chiesa, P., Martelli, E., Gallucci, F., Romano, M.C., Lozza, G., van Sint Annaland, M., 2015. Reactor design and operation strategies for a large-scale packed-bed CLC power plant with coal syngas. Int. J. Greenh. Gas Con. 36, 34-50.

Strohle, J., Orth, M., Epple, B., 2014. Design and operation of a 1MWth chemical looping plant. Appl. Energ. 113, 1490-1495.

Valverde, J.M., Perejon, A., Perez-Maqueda, L.A., 2012. Enhancement of fast CO2 capture by a nano-SiO2/CaO composite at Ca-looping conditions. Environ. Sci. Technol. 46, 6401‑6408.

Voldsun, M., Jordal, K., Anantharaman, R., 2016. Hydrogen production with CO_2 capture. Int. J. Hydrog. Energ.41, 4969-4992.

Vortmeyer, D., Berninger, R., 1982. Comments on the paper, theoretical prediction of effective heat transfer parameters in packed beds by Anthony Dixon and D. L. Cresswell [AIChE J., 25, 663 (1979)]. AIChE J. 28, 508-510.

Wolf, J., Yan, J., 2005. Parametric study of chemical looping combustion for tri-generation of hydrogen, heat, and electrical power with CO_2 capture. Int. J. Energy Res. 29, 739-753.

Xu, J., Froment, G.F., 1989. Methane steam reforming: II. Diffusional limitations and reactor simulation. AIChE J. 35, 97-103.

Zhenissova, A., Micheli, F., Rossi, L., Stendardo, S., Foscolo, P.U., Gallucci, K., 2014. Experimental evaluation of Mg- and Ca-based synthetic sorbents for CO_2 capture. Chem. Eng. Res. Des. 92, 727-740.

Zhou, Z., Han, L., Bollas, G.M., 2013. Model-based analysis of bench-scale fixed-bed units for chemical-looping combustion. Chem. Eng. J. 233, 331–348.

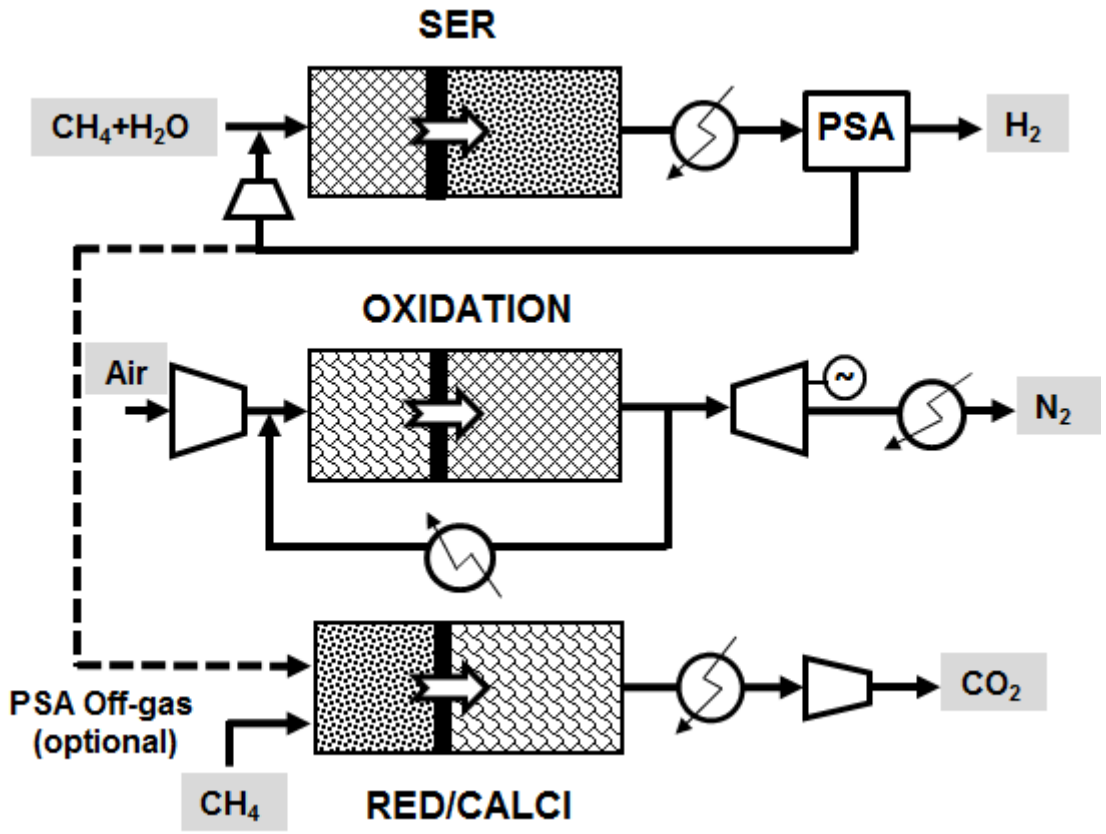

Fig. 1. Schematics of the calcium-copper chemical looping process in packed-bed reactors to produce separated streams of H_2, CO_2 and N_2.

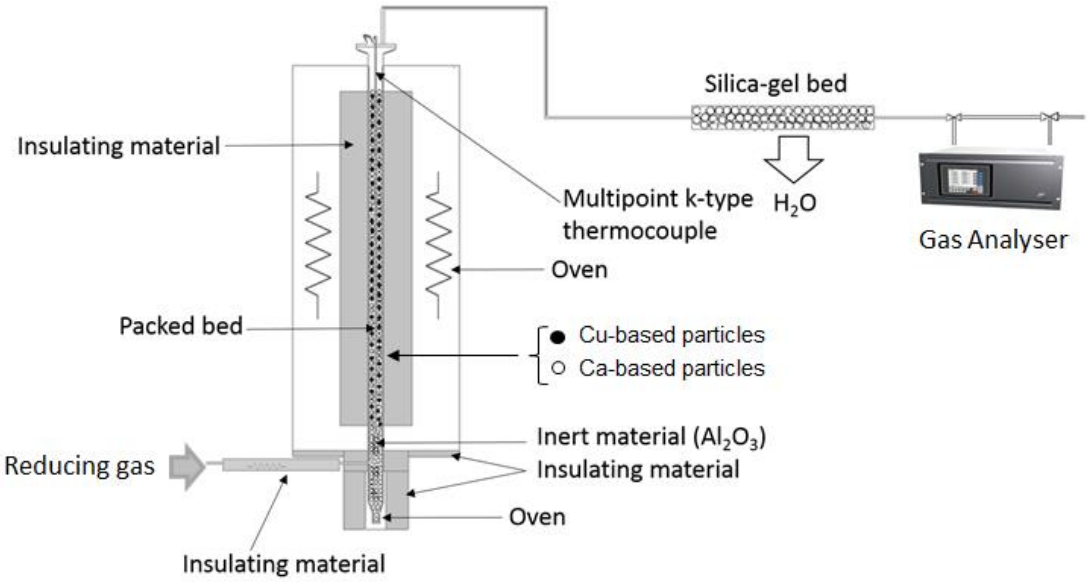

Fig. 2. Scheme of the experimental setup used in the reduction/calcination tests.

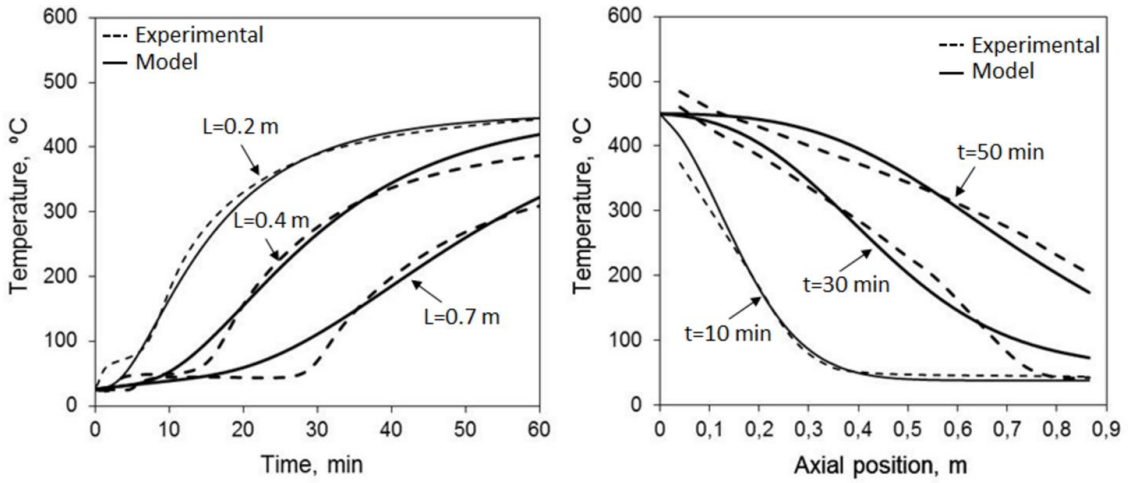

Fig. 3. Axial temperature profiles in the bed during the heating tests without any chemical reaction (starting solids temperature=25 ºC, inlet temperature=470 ºC, U=2.5 W/m^2K).

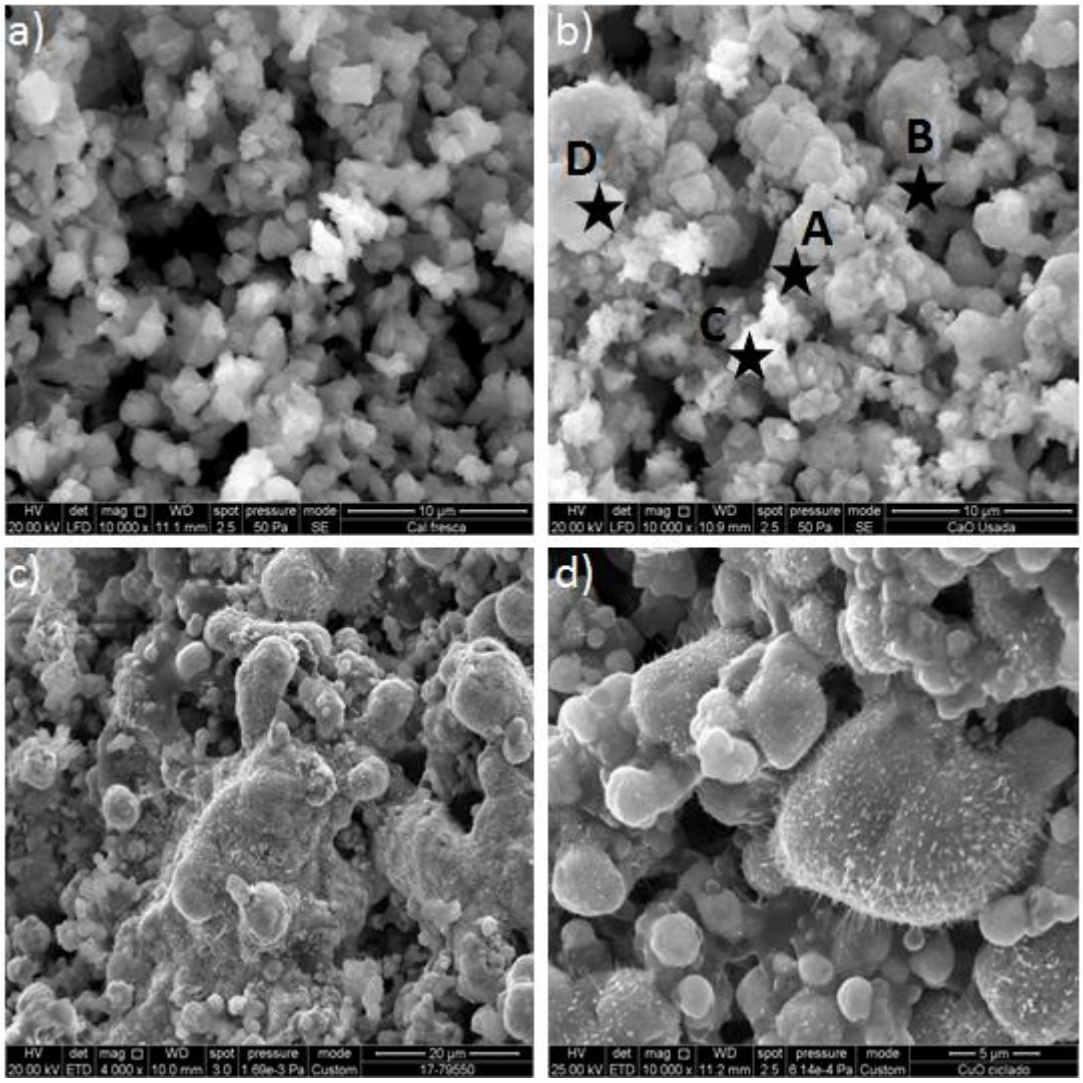

Fig. 4. SEM micrographs of the Ca-Cu based solids used in the fixed-bed reactor: a) initial CaO-based material, b) cycled CaO-based material, c) initial CuO-based solid, d) cycled CuO-based solid.

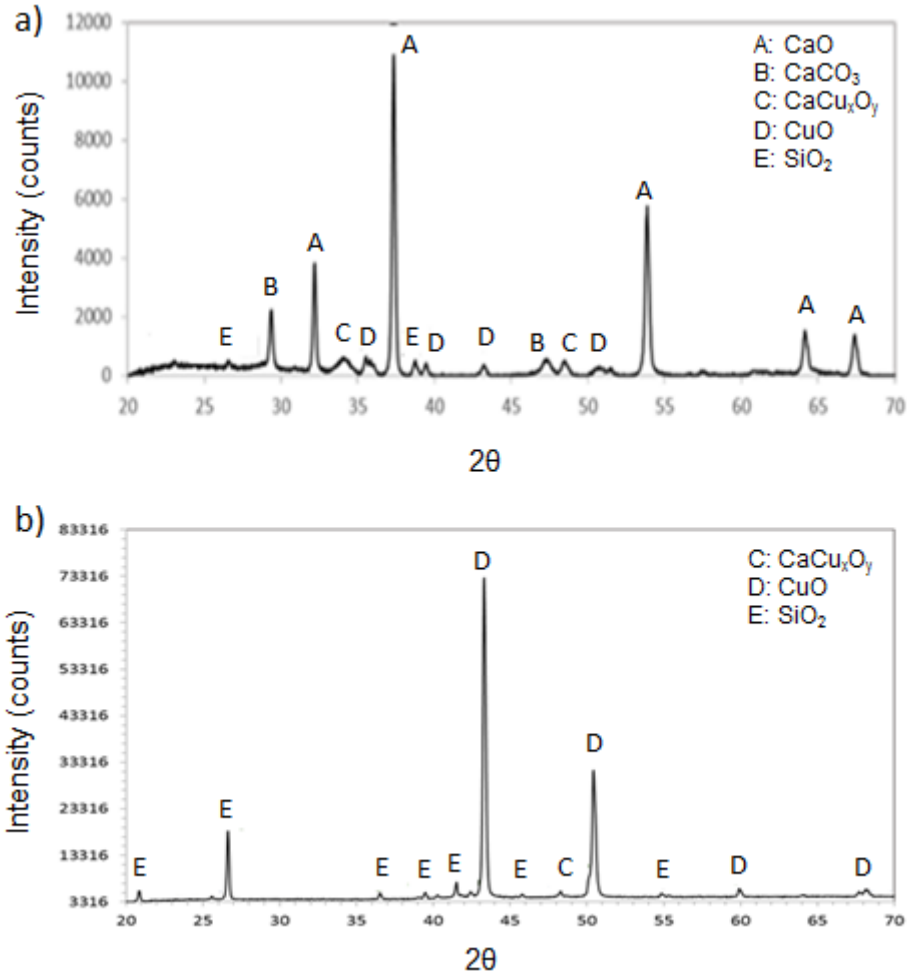

749

750 **Fig. 5.** XRD patterns of the a) CaO- and b) CuO-based materials after 25 cycles.

751

752

753

754

755

756

757

758

759

760

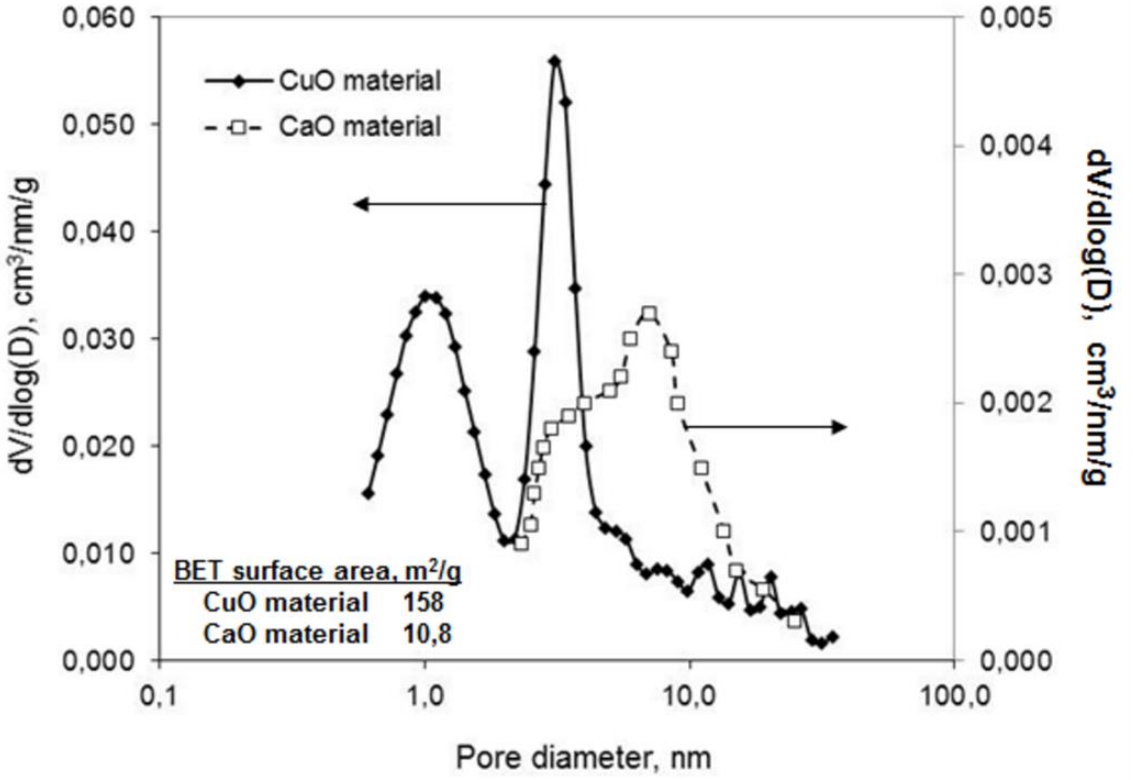

Fig. 6. Results obtained from the N_2 adsorption/desorption isotherms for fresh and cycled Ca-Cu solids.

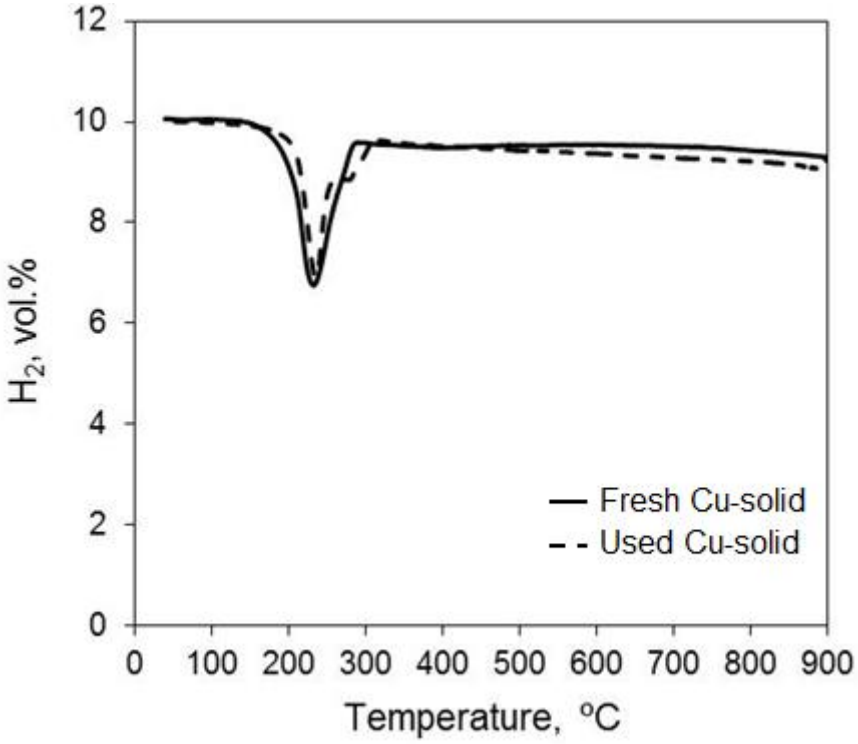

Fig. 7. Consumption of hydrogen during temperature-programmed reduction tests carried out with samples of fresh and used CuO-based samples.

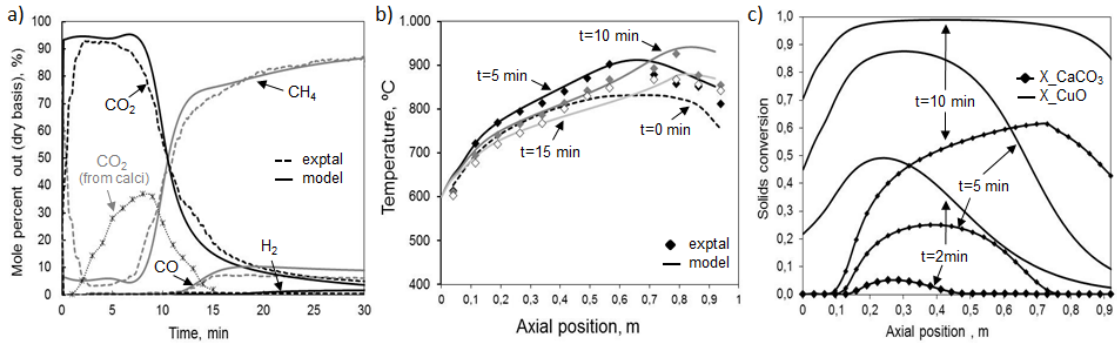

794

795 **Fig. 8.** Outlet gas composition, axial temperature profiles and theoretical solids
796 conversion profiles obtained during the test with methane (3 Nl/min in the feed, 760 ºC
797 of average starting bed temperature, cycle 1).

798

799

800

801

802

803

804

805

806

807

808

809

810

811

812

813

814

815

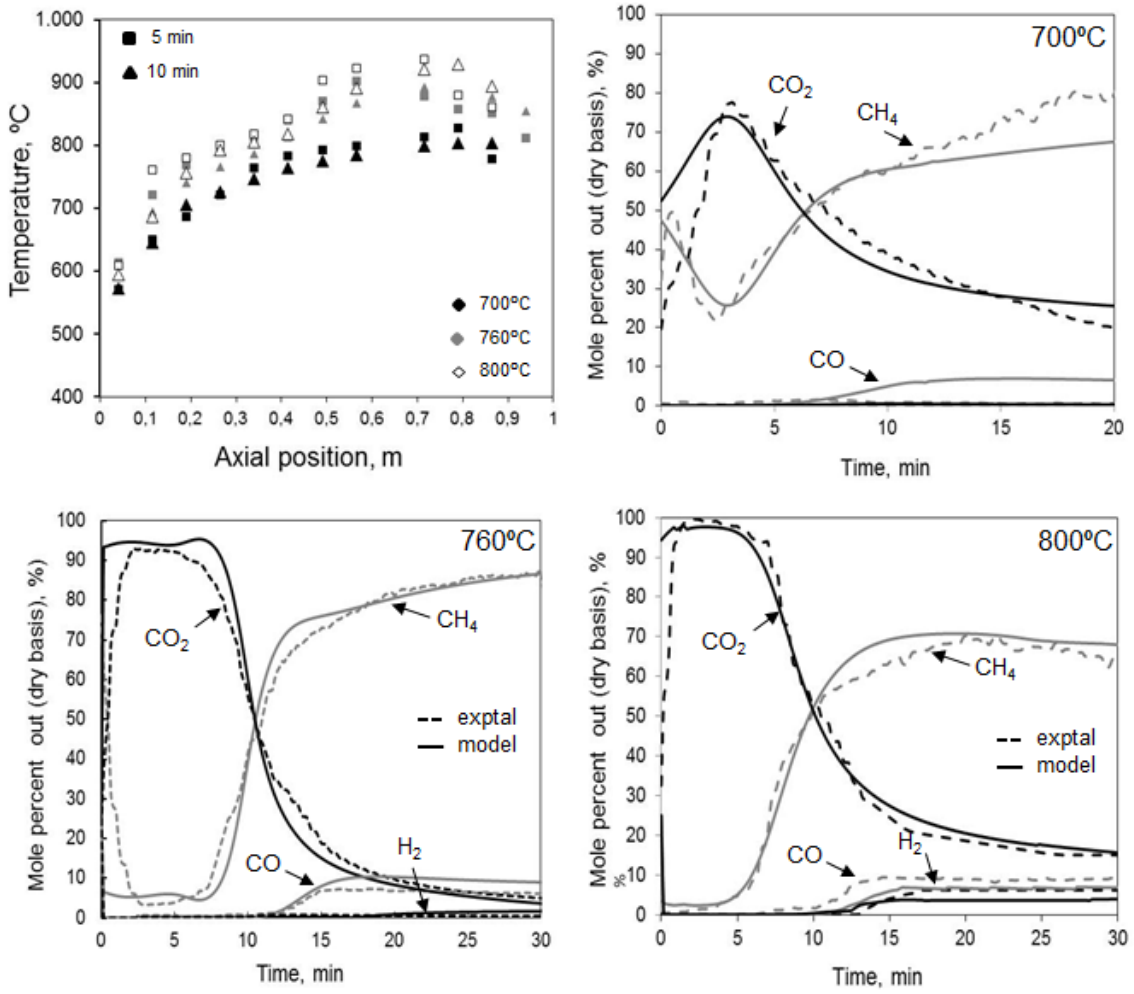

816

817 **Fig. 9.** Impact of the initial temperature of the solids on the reduction/calcination tests
818 with CH_4 (3 Nl/min of methane in the feed, cycles 2-4).

819

820

821

822

823

824

825

826

827

828

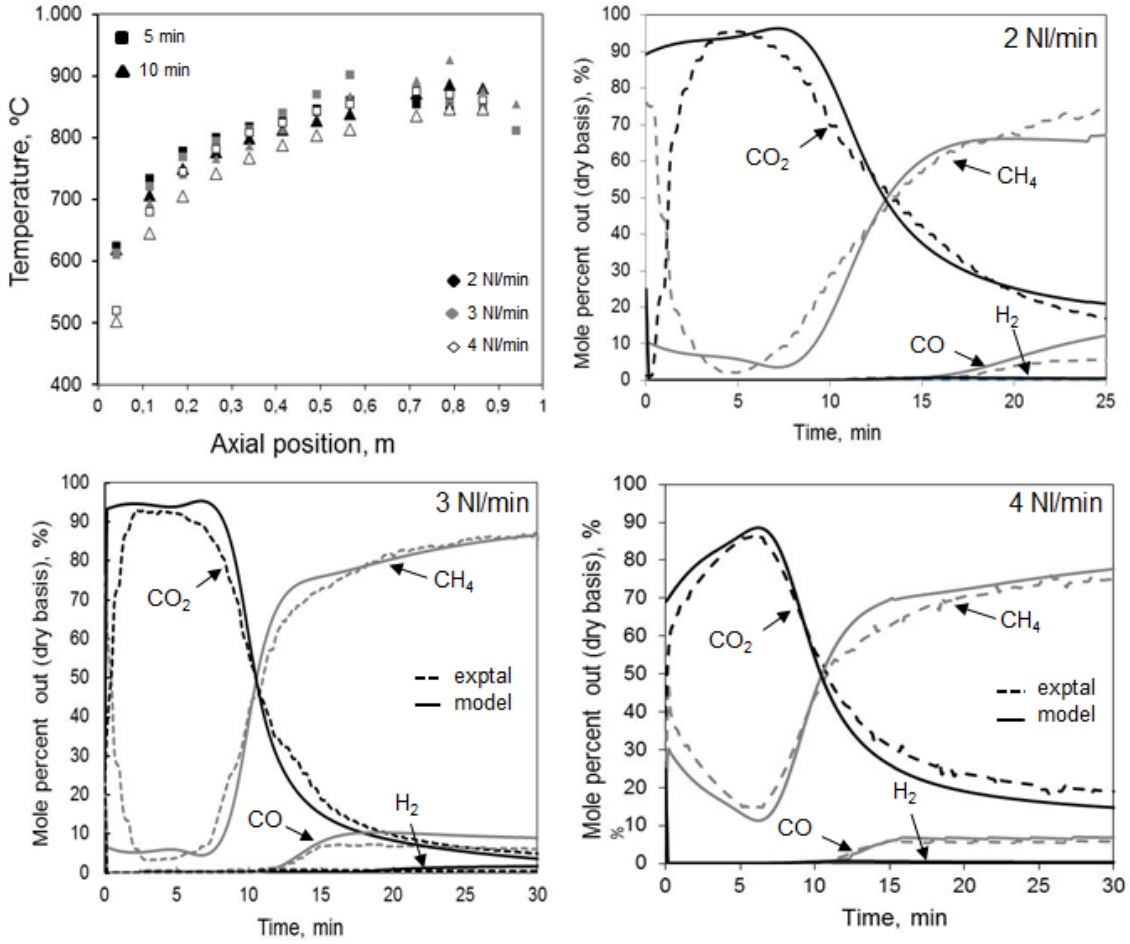

Fig. 10. Effect of the inlet gas flow rate on the reduction/calcination tests carried out with CH_4 (cycles 11-13).

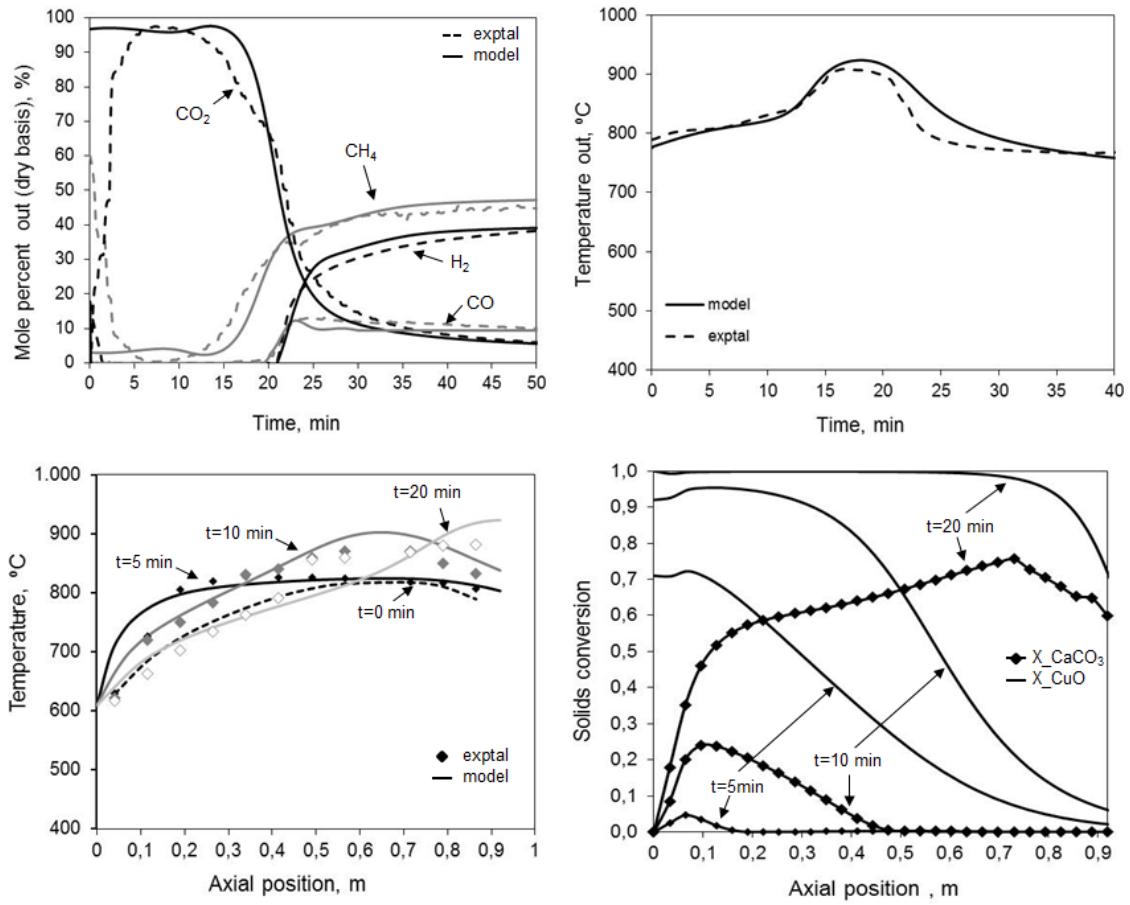

Fig. 11. Composition of the product gas, temperature and theoretical solids conversion profiles obtained during the reduction/calcination test with a mixture of methane and H_2 (50/50 vol.%), cycle 15.

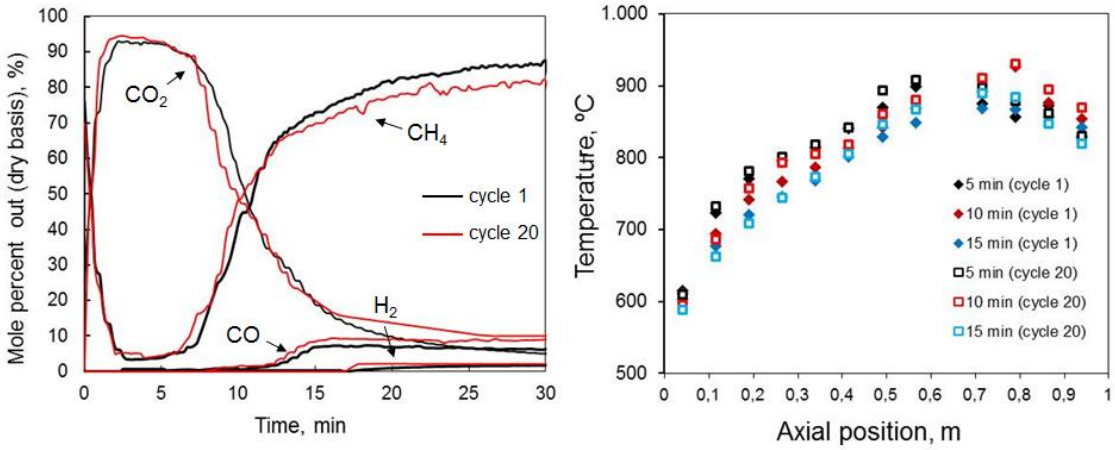

853

854 **Fig. 12.** Comparison of reactor performance in cycles 1 and 20 (3 Nl/min of CH_4 in the
855 feed, 760 ºC of average starting bed temperature).

856

857

858

859

860

861

862

863

864

865

866

867

868

869

870

871

872

873

874 **Table 1.** Equations to calculate the mass, energy and momentum balances and axial
875 dispersion.

Component mass balances

$$\varepsilon \frac{\partial C_i}{\partial t} = -u_g \frac{\partial C_i}{\partial Z} + \frac{\partial}{\partial Z}\left(D_{eff} \frac{\partial C_i}{\partial Z}\right) + \eta(1-\varepsilon)\rho ir_i$$

Energy balance

$$\left((1-\varepsilon)\rho_s C_{ps} + \varepsilon \rho_g C_{pg}\right)\frac{\partial T}{\partial t} = -u_g \rho_g C_{pg} \frac{\partial T}{\partial Z} + \frac{\partial}{\partial Z}\left(\lambda_{eff} \frac{\partial T}{\partial Z}\right) - \Sigma \eta_i (1-\varepsilon) H_{ri} \rho ir_i - U(4/Dr)(T - Tw)$$

Momentum balance

$$\frac{dP}{dZ} = -150 \frac{\mu_g u_g (1-\varepsilon)^2}{{d_p}^2 \varepsilon^3} + 1.75 \frac{\rho_g {u_g}^2 (1-\varepsilon)}{d_p \varepsilon^3}$$

Axial mass and heat dispersion coefficients (Edwards and Richarson, 1968; Vortmeyer and Berninger, 1982; Krupiczka, 1967; Gunn , 1978; Gunn and Misbah, 1993)

$$D_{eff} = \left[\frac{0.73}{R_e S_c} + \frac{0.5}{\varepsilon + \frac{9.7\varepsilon^2}{R_e S_c}}\right] u_g d_p$$

$$\lambda_{\text{eff}} = \lambda_{0\text{bed}} + \frac{\mathrm{R_e P_r k_g}}{\mathrm{Pe_{az}}} + \frac{{\mathrm{R_e}}^2 {\mathrm{P_r}}^2 {\mathrm{k_g}}^2}{6(1-\varepsilon)\mathrm{N_u}}; \quad \lambda_{0\text{bed}} = \left(\frac{\mathrm{k_s}}{\mathrm{k_g}}\right)^{0.28 - 0.757\log(\varepsilon) - 0.057\log\left(\frac{\mathrm{k_s}}{\mathrm{k_g}}\right)}$$

$$Pe_{az} = \frac{2p}{1-p}\ ; p = 0.17 + 0.29 e^{\left[\frac{-24}{R_e}\right]}; \quad N_u = 2 + 1.8 {R_e}^{0.5} {P_r}^{0.33}$$

876

877

878

879

880

881

882

883

884

885

886 **Table 2.** Kinetic equations assumed in the model.

CuO reduction (García-Labiano et al., 2004)

$$\frac{t}{\tau} = 1 - (1 - X_i)^{1/2} \qquad \tau = \frac{\rho_{m,i} L_i}{b k_i C_g^n}$$

$$r_i = \frac{\rho_i 1000}{M_i} \frac{dX_i}{dt}$$

Calcination of $CaCO_3$ (Martínez et al., 2012)

$$\frac{\mathrm{dX_{cal}}}{\mathrm{dt}} = \mathrm{k_{cal}}(1 - X_{cal})^{\frac{2}{3}} \left(\mathrm{C_{CO_{2,eq}}} - \mathrm{C_{CO_2}}\right); \; r_{cal} = \frac{\rho_{CaCO_3} 1000}{M_{CaCO_3}} \frac{dX_{cal}}{dt}$$

$$C_{CO_{2,eq}} = \frac{5.045\ x\ 10^{11}}{T} exp^{\left(\frac{-20.474}{T}\right)}$$

Kinetic parameters (García-Labiano et al., 2004; Martínez et al., 2012)

	CH_4	CO	H_2	Calcination
ρ_m, mol m^{-3}	80402	80402	80402	-
L_{Cu}, m	4.0 x 10^{-10}	4.0 x 10^{-10}	4.0 x 10^{-10}	-
k_{0i}, m s^{-1}	4.5 x 10^{-4}	5.9 x 10^{-6}	1.0 x 10^{-4}	252.02
E_{ai}, kJ mol^{-1}	60	14	33	91.7
b	4	1	4	-
n	1	1	1	-
η	0.1	0.2	0.2	1

Steam methane reforming and water gas shift (Xu and Froment, 1989)

$$\mathrm{r_1} = \frac{1}{(DEN)^2} \frac{k_1}{p_{H_2}^{2.5}} \left(\mathrm{p_{CH_4} p_{H_2O}} - \frac{\mathrm{p_{H_2}^3 p_{CO}}}{\mathrm{K_1}}\right)$$

$$\mathrm{r_2} = \frac{1}{(DEN)^2} \frac{k_2}{p_{H_2}^{3.5}} \left(\mathrm{p_{CH_4} p_{H_2O}^2} - \frac{\mathrm{p_{H_2}^4 p_{CO_2}}}{\mathrm{K_2}}\right)$$

$$\mathrm{r_3} = \frac{1}{(DEN)^2} \frac{k_3}{p_{H_2}} \left(\mathrm{p_{CO} p_{H_2O}} - \frac{\mathrm{p_{H_2} p_{CO2}}}{\mathrm{K_3}}\right)$$

$$\mathrm{DEN} = 1 + K_{CO}\mathrm{P_{CO}} + \mathrm{K_{H2}p_{H2}} + \mathrm{K_{CH4}P_{CH4}} + \mathrm{K_{H2O}}\frac{\mathrm{p_{H2O}}}{\mathrm{p_{H2}}}$$

Methane decomposition (Borguei et al. 2010)

$$\mathrm{r_4} = (\mathrm{k_4 p_{CH4}} - \frac{k_5}{k_6}\,\mathrm{p_{H_2}^2})/\left(1 + \frac{\mathrm{p_{H_2}^{3/2}}}{k_6}\right)^2$$

C gasification with H_2O and CO_2 (Snoeck et al., 2002)

$$\mathrm{r_5} = \frac{k_7}{K_{H2O}}\left(\frac{\mathrm{p_{H2O}}}{\mathrm{p_{H2}}} - \frac{\mathrm{p_{CO}}}{\mathrm{K_5}}\right) \Big/ \left(1 + \mathrm{k_{CH4}p_{CH4}} + \frac{\mathrm{p_{H2O}}}{\mathrm{p_{H2}}\,K_{H2O}} + \frac{\mathrm{p_{H_2}^{3/2}}}{K_{H2}}\right)^2$$

$$\mathrm{r_6} = \frac{k_8}{K_{CO}K_{CO2}}\left(\frac{\mathrm{p_{CO2}}}{\mathrm{p_{CO}}} - \frac{\mathrm{p_{CO}}}{\mathrm{K_{11}}}\right) \Big/ \left(1 + \mathrm{k_{CO}p_{CO}} + \frac{\mathrm{p_{CO2}}}{K_{CO}K_{CO2}\mathrm{p_{CO}}}\right)^2$$

Table 3. EDX Analyses of a sample of a used Ca-based solid (for which an SEM image is presented in Fig. 3b).

Element	Site A	Site B	Site C	Site D
O	60.8	13.7	35.2	60.4
Si	1.9	15.5	5.6	1.6
Ca	36.4	3.6	55.4	36.6
Cu	0.9	67.2	3.8	1.4